

7-1999

Examination of Beam Propagation in Misaligned Holographic Gratings and Comparison with the Acousto-optic Transfer Function Model for Profiled Beams

Monish Ranjan Chatterjee
University of Dayton, mchatterjee1@udayton.edu

David D. Reagan
State University of New York at Binghamton

Follow this and additional works at: https://ecommons.udayton.edu/ece_fac_pub

 Part of the [Computer Engineering Commons](#), [Electrical and Electronics Commons](#), [Electromagnetics and Photonics Commons](#), [Optics Commons](#), [Other Electrical and Computer Engineering Commons](#), and the [Systems and Communications Commons](#)

eCommons Citation

Chatterjee, Monish Ranjan and Reagan, David D., "Examination of Beam Propagation in Misaligned Holographic Gratings and Comparison with the Acousto-optic Transfer Function Model for Profiled Beams" (1999). *Electrical and Computer Engineering Faculty Publications*. 329.

https://ecommons.udayton.edu/ece_fac_pub/329

This Article is brought to you for free and open access by the Department of Electrical and Computer Engineering at eCommons. It has been accepted for inclusion in Electrical and Computer Engineering Faculty Publications by an authorized administrator of eCommons. For more information, please contact frice1@udayton.edu, mschlangen1@udayton.edu.

Examination of beam propagation in misaligned holographic gratings and comparison with the acousto-optic transfer function model for profiled beams

Monish R. Chatterjee

David D. Reagan

Binghamton University, SUNY
Department of Electrical Engineering
Binghamton, New York 13902-6000

Abstract. A transfer function formalism developed earlier for the propagation of profiled optical beams through acousto-optic Bragg cells is revisited and applied to a thick holographic grating. The results based on the holographic coupled wave model and the acousto-optic multiple scattering model are shown to be compatible, and equivalent parameters such as the Q and grating strength are defined for the two systems. Results for a Gaussian spatial profile are numerically computed and compared. For the holographic grating, a profiled beam may be interpreted as an angular misalignment or Bragg-angle mismatch problem. The case of Bragg-wavelength mismatch is also investigated for the case of a polychromatic READ beam with a uniform and a Gaussian amplitude spectrum. The resulting spatial amplitude distribution of the scattered order at the grating output is plotted as a function of the departure from the correct Bragg direction. © 1999 Society of Photo-Optical Instrumentation Engineers. [S0091-3286(99)00807-7]

Subject terms: acousto-optics; gratings; holography; profiled beams; polychromatic beams; Bragg diffraction.

Paper TCP-08 received Nov. 12, 1998; revised manuscript received Feb. 13, 1999; accepted for publication Feb. 16, 1999.

1 Introduction

Acousto-optic (A-O) and holographic gratings, though different in some fundamental aspects, have a number of common features. As thick gratings, both behave as Bragg-domain scatterers with similar amplitude characteristics. The basic analysis in both cases consists of the assumption that initially a planar, sinusoidal grating is formed (by a uniform plane wave of sound in the A-O case and the interference of two uniform plane waves of light with identical wavelengths in the holographic case). The scattered amplitudes are then evaluated readily from coupled equations with a perfectly Bragg-matched uniform plane wave READ beam. Many practical problems, however, deal with varying degrees of departure from the above ideal model, and attempts have been and continue to be made to accommodate more realistic grating formation or readout scenarios. Readout errors in a holographic grating occur due to non-Bragg READ beams. Drift in the wavelength of the READ beam or inaccuracies in aligning the beam to the target are common in certain environments. To determine changes in the efficiency and scattered direction as a function of input angular misalignment and/or wavelength detuning, we may consider changes in the wavelength or incident angle of the READ beam only, because the grating is fixed after recording. The terms $\Delta\lambda$ and $\Delta\theta$ that combine to form the dephasing parameter defined by Kogelnik¹ and subsequent researchers²⁻⁸ allow wavelength and angular deviations to be incorporated directly into the analysis of scattered amplitudes. In this paper, the behavior of holo-

graphic gratings under $\Delta\theta$ dephasing is examined from a transfer function perspective developed previously in the context of acousto-optic scattering of profiled beams based on plane wave multiple scattering formalism.⁹ In Sec. 2, the acousto-optic transfer function model for Bragg scattering of profiled beams is briefly reviewed and some numerical graphs presented for discussion. Kogelnik's model for a symmetrical, thick holographic grating is introduced in Sec. 3 and a detailed analysis presented for the corresponding transfer function model for profiled READ beams. To accomplish this, a parametric comparison is made of acousto-optic and holographic gratings. This accounts for angular misalignments only; and the resulting output profiles are compared with the corresponding acousto-optic problem. Efficiency variation under angular misalignment of a uniform plane wave is also considered in Sec. 3. The results of this approach are shown to be equivalent to Kogelnik's coupled wave theory. The effects of READ wavelength variations are investigated in Sec. 4 using polychromatic inputs in conjunction with previous findings relating output direction and input wavelength deviations. Section 5 concludes this paper.

2 The Transfer Function Formalism in Acousto-Optics for Profiled Light Beams

In an earlier work,⁹ a transfer function formalism was proposed that would enable direct representation of the scat-

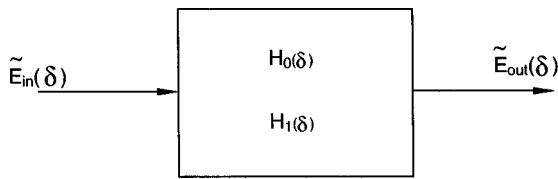


Fig. 1 Block diagram for sound–light interaction under a profiled READ beam.

tered amplitudes resulting from the propagation of a plane, arbitrary-profiled READ beam through an acousto-optic Bragg cell.

Representing the A-O setup as a linear system as shown in the schematic in Fig. 1, it is proposed that:

$$E_{out}(r) = \int_{-\infty}^{\infty} \tilde{E}_{in}(\delta) H(\delta) \exp[-j(2\pi/\lambda)\delta\phi_B r] \left(\frac{\phi_B}{\lambda}\right) d\delta, \tag{1}$$

where $\tilde{E}_{in}(\delta)$ is the angular spectrum of the profiled input beam $E_{in}(r)$, and the so-called plane wave transfer functions H_0 and H_1 take the form:

$$H_0(\delta) = \exp\left(-j\frac{\delta Q}{4}\right) \left\{ \cos \sqrt{\left(\frac{\delta Q}{4}\right)^2 + \left(\frac{\hat{\alpha}}{2}\right)^2} + \frac{j(\delta Q/4)\sin \sqrt{(\delta Q/4)^2 + (\hat{\alpha}/2)^2}}{\sqrt{(\delta Q/4)^2 + (\hat{\alpha}/2)^2}} \right\}, \tag{2}$$

and

$$H_1(\delta) = -j\frac{\hat{\alpha}}{2} \exp\left(j\frac{\delta Q}{4}\right) \frac{\sin \sqrt{(\delta Q/4)^2 + (\hat{\alpha}/2)^2}}{\sqrt{(\delta Q/4)^2 + (\hat{\alpha}/2)^2}}, \tag{3}$$

where $\hat{\alpha}$ is the peak phase shift of the light beam as it traverses the grating, $\delta\phi_B$ is a measure of the angular deviation of an input plane wave from the exact Bragg angle ϕ_B , and Q (a grating figure-of-merit that defines Bragg or Raman–Nath operation) is the well-known Klein–Cook parameter. At this stage, it is meaningful to discuss some of the similarities and distinctions between the A-O and holographic gratings some of whose characteristics under non-Bragg conditions are compared in this paper. An acousto-optic grating operates^{10–12} in either of two regimes—the Bragg (thick gratings, $Q > 2\pi$) or the Raman-Nath (thin gratings, $Q \rightarrow 0$). The discussion in this paper is limited to relatively thick gratings for both the holographic and the A-O cases. Holographic gratings are generally under no restrictions regarding the physical size of the input angle of either the WRITE or the READ beams. Acousto-optic gratings, however, are limited to operation at relatively small input angles due to the large difference in wavelengths between light and sound. Hence, if any meaningful comparisons are to be made, the Bragg angle must be limited to relatively small values for the analysis of both the acousto-optic and the holographic gratings. Using the Fourier transform formalism in Eq. (1), it is now possible to evaluate the output beam profiles for both the zeroth and first order

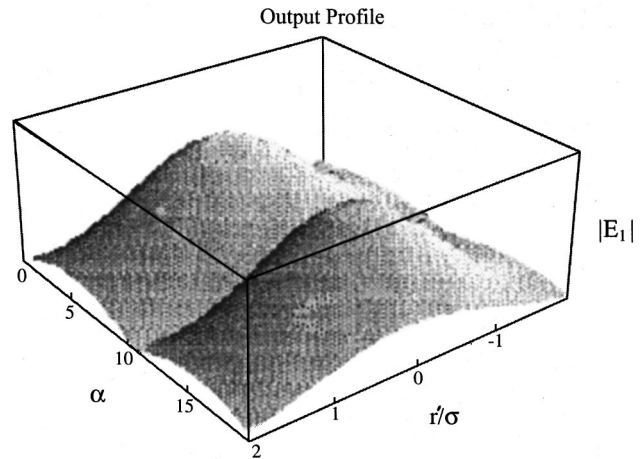


Fig. 2 First order E_1 versus $\hat{\alpha}$ and r'/σ (where σ is the READ beam width) for $Q=20$.

beams (corresponding to the R and S beams, respectively, to be discussed later for holographic gratings) for arbitrary plane wave input profiles. The formalism was successfully applied to evaluate⁹ the scattered outputs for Gaussian READ beam profiles under conditions of varying $\hat{\alpha}$.

From Figs. 2 and 3, which show the evolution of the scattered field E_1 with $\hat{\alpha}$ and the normalized radial coordinate (r') for a Q of 20 and 533, respectively, it is evident that under certain conditions a lateral shift occurs in the radial direction of the E_1 field amplitude. As $\hat{\alpha}$ increases for a given Q , the radial shift in the E_1 beam increases. It has been shown⁹ that the E_0 beam (not shown here) does not experience any radial shift until $\hat{\alpha}$ exceeds $\pi/2$, after which point the shift appears to be linearly dependent on any further changes in $\hat{\alpha}$.

The above-mentioned shift observed in the plots of the grating outputs has a limiting value, determined by certain parameters of the grating. The grating strength is determined by the value of the modulation index for holographic gratings and by the sound pressure for acousto-optic gratings. As the grating strength increases, the shift increases,

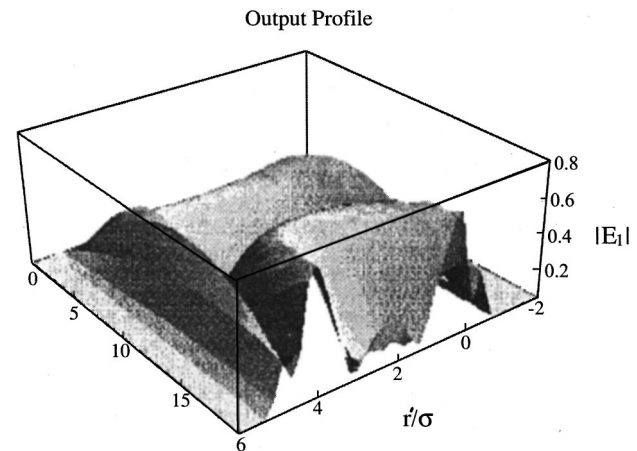


Fig. 3 First order E_1 versus α and r'/σ (where σ is the READ beam width) for $Q=533$.

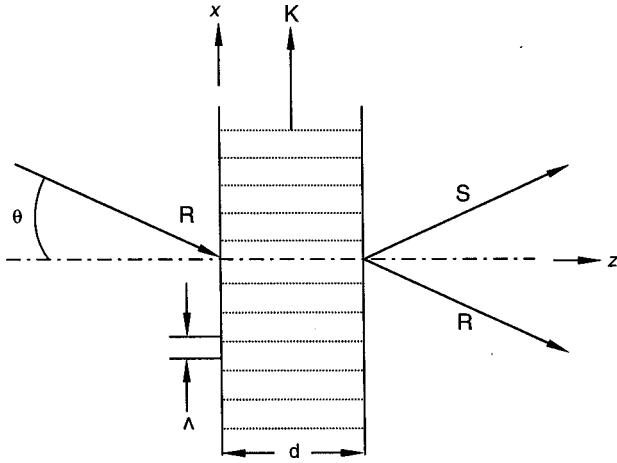


Fig. 4 Schematic for holographic grating readout.

until this limiting value is reached, after which any further increases in ν (holographic phase delay) or $\hat{\alpha}$ (acousto-optic case) have no effect on the amount of the lateral shift. These limiting values have been derived for acousto-optic gratings⁹ as $\hat{\alpha}$ approaches infinity. The expressions are:

$$E_1(r)|_{\hat{\alpha} \rightarrow \infty} \approx \frac{-jE_{\text{inc}}\Gamma(1)\sin(\hat{\alpha}/2)}{\sigma_1\sqrt{2\pi}} \times \exp\left[-\frac{1}{2\sigma_1^2}\left(r + \frac{Q\Lambda}{4\pi}\right)^2\right], \quad (4)$$

$$E_0(r)|_{\hat{\alpha} \rightarrow \infty} \approx E_{\text{inc}} \left\{ \frac{\Gamma(1)\cos(\hat{\alpha}/2)}{\sigma_1\sqrt{2\pi}} - \frac{Q\lambda^3\Gamma(2)[(Q/4) + (\pi/\Lambda)r]\sin(\hat{\alpha}/2)}{16\sqrt{2}\pi^{5/2}\sigma_1^3\phi_B^3\hat{\alpha}\Lambda} \right\} \times \exp\left[-\frac{1}{2\sigma_1^2}\left(r + \frac{Q\Lambda}{4\pi}\right)^2\right]. \quad (5)$$

Both of the above equations indicate a maximum radial shift of $-(Q\Lambda/4\pi)$ when the grating strength (or sound pressure in acousto-optics) is increased to infinity. Hence,

$$\lim_{\hat{\alpha} \rightarrow \infty} r_{\text{Acousto}} \rightarrow -\frac{Q\Lambda}{4\pi}. \quad (6)$$

3 Holographic Gratings: The Kogelnik Model and the Transfer Function Formalism

A holographic grating is formed by the interference of two light beams, viz., the reference beam (also called the regular or R beam) and the object (also called the scattered or S beam) on a photosensitive material (such as photographic emulsions, gelatins, or photorefractive and other volume media). This grating may then be read by a single beam (usually the reference beam), thus reconstructing both the regular and the scattered beams at the output. The basic geometry of Kogelnik's analysis is shown in Fig. 4. For the

unslanted, symmetrical grating shown, upon read out with a unit amplitude, uniform and planar R beam, the scattered S and R fields are given by¹:

$$S = -j\nu\sqrt{\frac{c_r}{c_s}} \exp\left(-j\frac{\vartheta d}{2c_s}\right) \frac{\sin\sqrt{\nu^2 + (\vartheta d/2c_s)^2}}{\sqrt{\nu^2 + (\vartheta d/2c_s)^2}}, \quad (7)$$

$$R = -\sqrt{\frac{c_r}{c_s}} \times \exp(j\xi) \frac{\sqrt{\nu^2 + \xi^2} \cos\sqrt{\nu^2 + \xi^2} - j\xi \sin\sqrt{\nu^2 + \xi^2}}{\sqrt{\nu^2 + \xi^2}},$$

$$\vartheta = \frac{\beta^2 - \sigma^2}{2\beta} = -\Delta\theta K \sin\theta_B - \frac{\Delta\lambda K^2}{4\pi n} \quad (8)$$

where

- ϑ = the dephasing parameter
- ν = a phase delay factor
- $\xi (= \vartheta d/2c_s)$ = a dimensionless dephasing factor
- $\Delta\theta$ and $\Delta\lambda$ = the angular and wavelength deviations of the READ beam from the Bragg angle
- θ_B = the Bragg angle
- d = the grating thickness
- K = the magnitude of the "grating vector"
- c_R = the direction cosine of the R beam
- c_S = the direction cosine of the S beam.

3.1 Application of the Transfer Function Formalism

As established for the A-O problem for profiled READ beams, if a transfer function could be defined for the grating, then a knowledge of the (angular) spectral characteristics of the input signal would enable determination of the output fields of this (linear) system. Thus, the output beam profile of the grating would be the convolution of the READ beam profile and the "spatial impulse response" of the grating. Alternatively, the product of the Fourier transform of the input profile and the transfer function of the grating would yield the angular spectrum of the output, which in principle may be inverse Fourier transformed to provide the output beam spatial profile.¹³ The effects of any variations in input angle (such as a misaligned input beam) may be evaluated using this method. The transfer functions and impulse responses used in this section were derived by direct comparison with the acousto-optic transfer functions first presented earlier. They are shown to be entirely compatible with the formalism derived on the basis of the multiple plane wave formalism in acousto-optics.⁹ To simplify the analysis for the holographic case, it is assumed that (1) the READ beam enters the holographic medium from air and exits the grating into air, thus eliminating any angular changes due to Snell's law; (2) the loss due to absorption is negligible; (3) the light waves are linearly polarized in the same (perpendicular) direction for every case considered;

(4) the grating is unslanted and symmetrical; and (5) the grating is thick (i.e., the operation is at or near Bragg).

If we consider the situation in which the wavelength is unperturbed but there is a spread of slightly misaligned input angles, the grating transfer functions may then be determined as functions of the angular misalignment $\Delta\theta$ (where the latter may have a spread according to the angular spectrum of a profiled READ beam). In the complementary case, where the incident angle θ is constant but there is wavelength detuning, the dependence on $\Delta\lambda$ over a range of non-Bragg-matched wavelengths (such as for a polychromatic beam) cannot, strictly speaking, be described in terms of a beam profile, because a spatial beam profile presupposes a monochromatic wave.¹³ This is discussed in more detail later, along with an alternative approach to investigating this problem. The $\Delta\theta$ case will be approached first, by simply setting $\Delta\lambda$ to zero in Eqs. (7) and (8). This results in the following expressions for the S and R beam transfer functions (after dividing the uniform plane wave scattered amplitudes by the READ beam amplitude):

$$H_S(\Delta\theta) = -j\nu \sqrt{\frac{c_r}{c_s}} \exp\left(-j \frac{\Delta\theta K \sin \theta_B d}{2c_s}\right) \times \frac{\sin \sqrt{\nu^2 + (\Delta\theta K \sin \theta_B d / 2c_s)^2}}{\sqrt{\nu^2 + (\Delta\theta K \sin \theta_B d / 2c_s)^2}}, \quad (9)$$

$$H_R(\Delta\theta) = \sqrt{\frac{c_r}{c_s}} \exp\left(j \frac{\Delta\theta K \sin \theta_B d}{2c_s}\right) \times \left\{ \cos \sqrt{\nu^2 + \left(\frac{\Delta\theta K \sin \theta_B d}{2c_s}\right)^2} - \left(\frac{\Delta\theta K \sin \theta_B d}{2c_s}\right) \frac{j \sin \sqrt{\nu^2 + (\Delta\theta K \sin \theta_B d / 2c_s)^2}}{\sqrt{\nu^2 + (\Delta\theta K \sin \theta_B d / 2c_s)^2}} \right\}. \quad (10)$$

Using the transfer functions presented above, the scalar output field profile in both the r and k domains (k implying spatial frequency or wavenumber) may be determined. As before, we define the input fields and their angular spectra in terms of their Fourier pairs:

$$\tilde{E}(\Delta\theta) = 2\pi \int_{-\infty}^{\infty} E(r) \exp\left(j \frac{2\pi}{\lambda} \Delta\theta r\right) dr = f\{E(r)\}, \quad (11)$$

$$E(r) = \int_{-\infty}^{\infty} \tilde{E}(\Delta\theta) \exp\left(-j \frac{2\pi}{\lambda} \Delta\theta r\right) d\left(\frac{\Delta\theta}{\lambda}\right) = f^{-1}\{\tilde{E}(\Delta\theta)\}, \quad (12)$$

where f and f^{-1} signify the forward and inverse Fourier transforms, respectively. We must keep in mind that the current work concerns the read out of holographic gratings illuminated by profiled READ beams (which incorporates the case of READ angular misalignment).

Table 1 Parametric comparison of acousto-optic and holographic gratings.

Acousto-Optic	Holographic
$\hat{\alpha}/2$	ν
$C A $	$1/\sqrt{C_R C_S}$
$-\delta(\theta_B)$	$\Delta\theta$
$-\delta Q/4$	ξ
L	d
$ Q $	$2Kd\theta_B$

Analogous to Eq. (1), the spatial output profile may now be expressed as the inverse Fourier transform of the product of the transfer function and the angular spectrum of the input:

$$E_{out}(r) = f^{-1}\{\tilde{E}(\Delta\theta)H(\Delta\theta)\} = \int_{-\infty}^{\infty} \tilde{E}(\Delta\theta)H(\Delta\theta) \exp\left(-j \frac{2\pi}{\lambda} \Delta\theta r\right) d\left(\frac{\Delta\theta}{\lambda}\right). \quad (13)$$

In the above analyses, we have considered only lossless and unslanted holographic and acousto-optic gratings illuminated with uniform plane waves. By comparing the transfer functions for the two cases as defined by Eqs. (2), (3), (9), and (10), we arrive at the correspondence between the parameters of the two systems as listed in Table 1. The equivalence of the two systems is evident from the table, and it is apparent that one may define a Q parameter for holographic gratings as is done for acousto-optic gratings. Incidentally, such a Q parameter was defined and its properties investigated earlier by Magnusson et al. for thick gratings.¹² As was done for the A-O case, the use of the fast Fourier transform (FFT) made it possible to obtain numerical solutions for the case of a Gaussian-profile READ beam and plot the results, some of which are presented later in this section. Remember that the output profiles may be evaluated for READ beams with any arbitrary profile using the above formalism. For the Gaussian READ beam profile, the plots that follow consider a grating whose parameters are typical of a thick holographic grating. We thus assume:

$$\begin{aligned} \theta_B &= 0.5236 \text{ rad} = 30 \text{ deg} \\ d &= 0.7958 \text{ mm} \\ \lambda &= 1 \mu\text{m} \\ \Lambda &= 1 \mu\text{m} \\ \text{beam waist radius } \sigma &= 1 \text{ mm.} \end{aligned}$$

Plots of the S beam output as a function of ν and r/σ are shown in Figs. 5 and 6 for $Q=5,000$ and $50,000$ respectively. As can be seen, at the low value of Q , the beam emerges with little distortion, while at a Q which is ten times higher, it becomes highly distorted. This effect may be explained from the convolution perspective in that at a low Q , the impulse response of the grating looks closer to an impulse and thus permits the input profile to emerge undistorted. At a higher Q , however, the impulse response widens, and the input appears more impulselike to the grat-

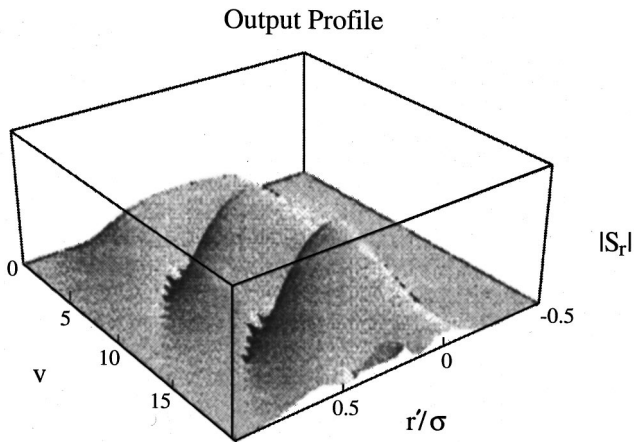


Fig. 5 The S output for $Q=5000$, $\theta_B=30$ deg.

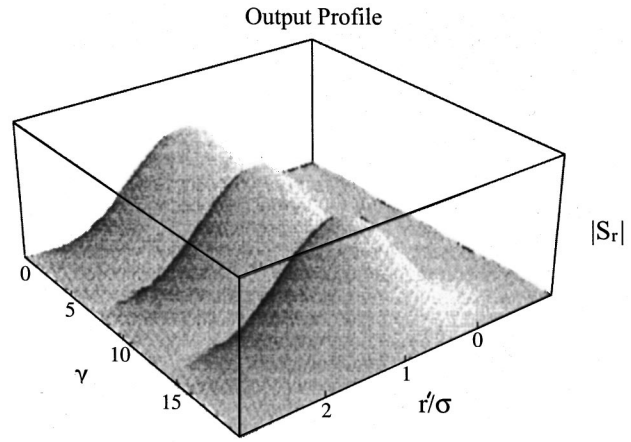


Fig. 7 The S beam output for $Q=20$, $\theta_B=0.005236$ deg.

ing. Hence the output begins to resemble the impulse response of the grating. This conjecture is readily verified by plotting the grating impulse response separately. We may note here that the above plots involved a typical thick holographic grating with a Bragg angle of 30 deg, resulting in Q of 5000 or more. For comparison of the holographic transfer function with that obtained for the A-O case, it is necessary to choose holographic parameters that will ensure comparable Q values. This requirement is satisfied by choosing a small Bragg angle (0.005236 rad), even though it is quite atypical for a holographic grating. The above further requires that the wavelength of the READ beam be kept considerably smaller than the grating spacing (which is set at one tenth the standard deviation or width of the Gaussian beam, i.e., $\sigma/10$). In Figs. 7 through 10, the output profiles of both the R and S beams are shown, plotted against both the radial distance and grating strength. For such a hypothetical holographic grating, the plots should be contrasted with Figs. 2 and 3 for an A-O grating to arrive at an understanding of the similarities and differences between the two grating types. Particular attention should be paid to the amount of radial shift for a particular value of ν or $\hat{\alpha}$, for a fixed Q . The degree and shape of the distortion present at high Q and grating strengths are also important features. As expected, the plots are similar in virtually all

respects except that additional cycles are in the holographic plots due to the relationship $\nu = \hat{\alpha}/2$, where both parameters have been varied in the range 0 through 20 in the plots. The radial spatial shifts in the holographic case are also apparent from both the realistic graphs in Figs. 5 and 6, and the simulated graphs in Figs. 7 through 10. In this context, it is meaningful to note that to see lateral shifts in the direction of the output beam, using typical holographic gratings, whose grating period is on the order of the input wavelength, the Q must be dramatically higher than that required for the same amount of shift from an A-O grating. When the assumptions under which acousto-optic gratings operate (small Bragg angle, large grating spacing) are applied to holographic gratings, however, there is a pronounced shift at Q levels comparable to those encountered using acousto-optic gratings. We may also note that as Q decreases, the width of the grating's impulse response decreases. Due to the inverse relationship between impulse response and transfer function, therefore, the output looks more like the input at low Q , implying that the impulse response of the system looks more and more like a delta function. As discussed before, at higher Q the output looks more like the impulse response of the system because the input appears more impulselike in this case.

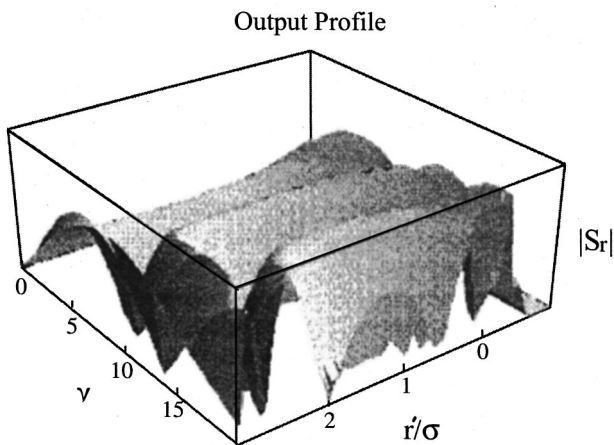


Fig. 6 The S output for $Q=50,000$, $\theta_B=30$ deg.

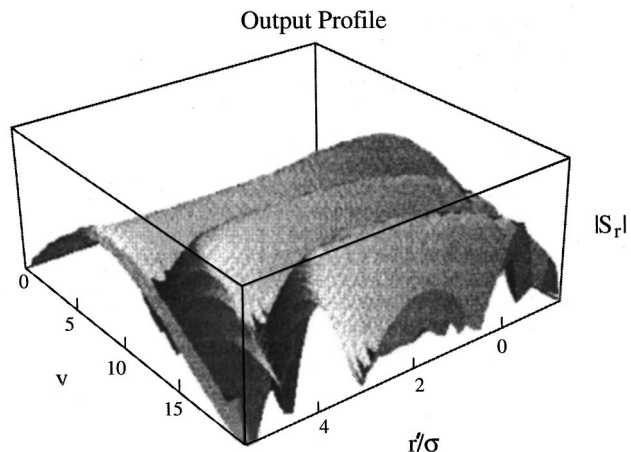


Fig. 8 The S beam output for $Q=533$, $\theta_B=0.005236$ deg.

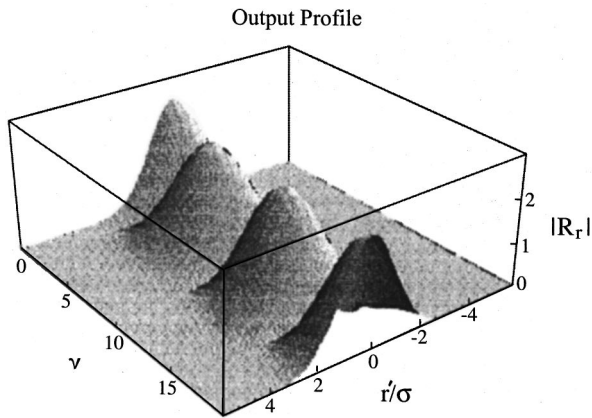


Fig. 9 The R beam output for $Q=20$, $\theta_B=0.005236$ deg.

For holographic gratings, as the grating strength (ν) increases for a given Q , we find that the distortion of the R beam at the output increases. Curiously, for the S beam, significant distortion only arises when ν is less than $\pi/2$. For grating strengths greater than this value, it worsens only with increases in Q and is independent of the grating strength. But Q and ν are both responsible for shifts in the radial output direction of the beam, which are opposite in character, compared to the distortion problem. As ν increases for a given Q , the shift in the S beam output increases. The R beam, however, experiences no shift until the grating strength is greater than $\pi/2$, after which point the shift appears to be linearly dependent on any further changes in ν . These properties are evident in the graphs shown in Figs. 2, 3, and 7 through 10. Thus, in the limit as $\theta_B \rightarrow 0$, we may conclude that thick A-O and holographic gratings are essentially similar in nature.

3.2 Efficiency Under Angular Dephasing

Sometimes, we need to know how nonideal conditions such as inaccuracies (i.e., a profile, or a simple angular mismatch) in the READ beam affect the performance of the grating. For a Bragg grating with two significant orders, the efficiency corresponding to a single uniform plane wave input is simply given by:

$$\eta = |S|^2, \tag{14}$$

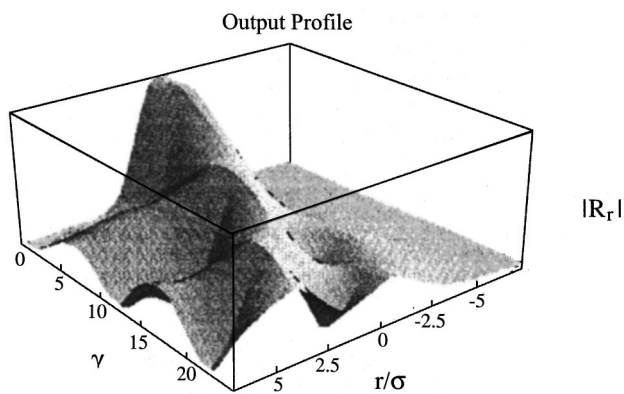


Fig. 10 The R beam output for $Q=533$, $\theta_B=0.005236$ deg.

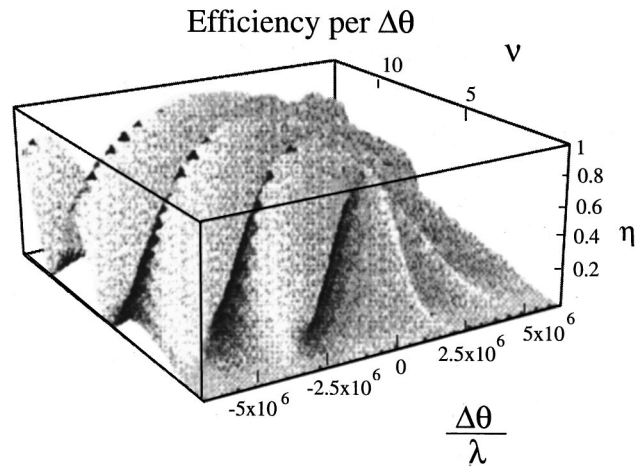


Fig. 11 Holographic efficiency vs angular misalignment and grating strength for $Q=20$.

where $|S|^2$ is the intensity of the scattered output beam, which after substituting $\xi = Q\Delta\theta/4\theta_B$ becomes

$$\eta = \frac{\nu^2}{[\nu^2 + (Q\Delta\theta/4\theta_B)^2][1 + \cot^2 \sqrt{\nu^2 + (Q\Delta\theta/4\theta_B)^2}]} \tag{15}$$

(The efficiency corresponding to a single uniform plane is the only definition we follow here; we do not define any composite “profile” or “spectral” efficiency.) Plots of efficiency versus grating strength and angular misalignment are shown in Figs. 11 and 12 for $Q=20$ and 533, respectively. From the plots it is clear that the nature of variation in efficiency versus input angular error is essentially the same regardless of Q . While the basic shape does not change with Q , only the range of angles over which the efficiency remains significant. This implies that Q may be regarded as an indicator of angular selectivity. Also notable are the periodicity of the efficiency and the concave nature of the curves as ν increases above π .

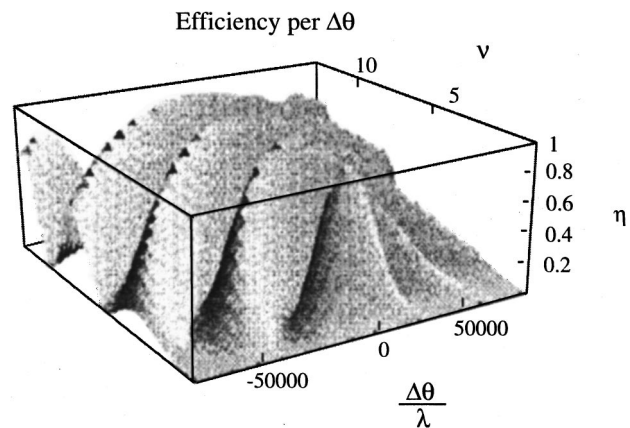


Fig. 12 Holographic efficiency vs angular misalignment and grating strength for $Q=533$.

4 Output Amplitude Distribution and Angular Spread for Polychromatic READ Beams

Suppose we consider next the case of a READ beam wavelength error (assuming a Bragg-matched incident angle). The scattered amplitudes of the grating may then be determined as functions of the wavelength detuning $\Delta\lambda$. However, they may be evaluated only as responses to discrete plane wave inputs to the system, the notion of a spatial profile being incompatible with a wavelength distribution (such as for a polychromatic input). This is accomplished by setting $\Delta\theta$ to zero and evaluating the output response in terms of $\Delta\lambda$ (the converse of the situation described above). If the R beam is used to read the grating, the following equations apply:

$$S(\Delta\lambda) = -j \sqrt{\frac{c_r}{c_s}} \exp\left(-j \frac{\Delta\lambda K^2 d}{8\pi n c_s}\right) \times \frac{\sin\sqrt{\nu^2 + (\Delta\lambda K^2 d/8\pi n c_s)^2}}{\sqrt{\nu^2 + (\Delta\lambda K^2 d/8\pi n c_s)^2}} R_{in}, \quad (16)$$

$$R(\Delta\lambda) = \sqrt{\frac{c_r}{c_s}} \exp\left(j \frac{\Delta\lambda K^2 d}{8\pi n c_s}\right) \times \left\{ \cos\sqrt{\nu^2 + (\Delta\lambda K^2 d/8\pi n c_s)^2} - \frac{\Delta\lambda K^2 d}{8\pi n c_s} \frac{j \sin\sqrt{\nu^2 + (\Delta\lambda K^2 d/8\pi n c_s)^2}}{\sqrt{\nu^2 + (\Delta\lambda K^2 d/8\pi n c_s)^2}} \right\} R_{in}, \quad (17)$$

where R_{in} is the READ beam input amplitude.

Note that the $\Delta\lambda$ -dependent expressions cannot be subjected to the usual spatial Fourier transform, because the latter involves space and angle at a fixed wavelength. Thus, the $\Delta\theta/\lambda$ -dependent expressions derived earlier for profiled beams had an inverse association with r , making them k -domain relationships, and as such they could be viewed as transfer functions. Now, even though a comparable transfer function formalism cannot be derived for the polychromatic problem, an output amplitude distribution can nevertheless be achieved using an input whose wavelength varies. Thus, plane waves with differing wavelengths can be introduced to the input of the grating individually. It has been determined¹⁴ that each input wavelength other than the Bragg wavelength will result in an angular deviation at the output. Also, using Eqs. (16) and (17), the amplitude of each of these deviated beams can be determined. So, if we have a specific output angle and an amplitude associated with that angle, we have a spatial amplitude distribution. This spatial distribution cannot strictly be called a profile, however, because it is not monochromatic. If, however, the wavelength spread is very small, it may be useful, for practical purposes, to treat it as a profile. Even so, it must be stressed that the Fourier transform or the inverse Fourier transform of such an entity would have no real meaning, due to its nonmonochromatic nature. To find the angle at which the beam exits the grating, we use the result¹⁴:

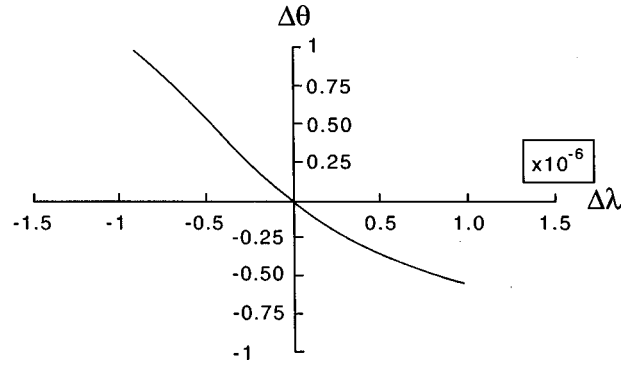


Fig. 13 Output angular error versus READ beam wavelength error (after Ref. 14).

$$\Delta\theta_{out} = - \left\{ \tan^{-1} \left[\left(1 + 2 \frac{\Delta\lambda}{\lambda} \right) \tan(\theta_B) \right] - \theta_B \right\}. \quad (18)$$

The assumptions in deriving Eq. (18) are:

1. The operation is near-Bragg.
2. The wavelength error $\Delta\lambda$ is relatively small.

The fractional wavelength error should preferably be about 10% or less; however, in many cases, slightly higher variations are within acceptable tolerances. Figure 13 shows a plot of the output angular error versus the READ wavelength error at a Bragg angle of 30 deg.

To find the output spatial amplitude distribution corresponding to a READ wavelength spectrum, we first consider a READ input with a uniform distribution of amplitude versus wavelength. Effectively, this implies that a series of plane waves (each with a different wavelength and unit amplitude) is incident at the grating input at the Bragg angle. Such a distribution is shown in Fig. 14, where the center (or Bragg) wavelength is 1 μm and the wavelength spread is kept within 30% of the center wavelength in either direction. The following parameters are also assumed:

- $\theta_B = 0.5236 \text{ deg}$
- $Q = 5000$
- $d = 795.8 \mu\text{m}$
- $\lambda = \Lambda = 1 \mu\text{m}$.

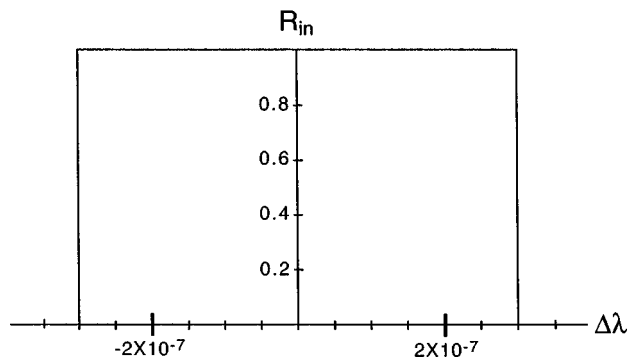


Fig. 14 Uniform amplitude spectrum for a polychromatic READ beam.

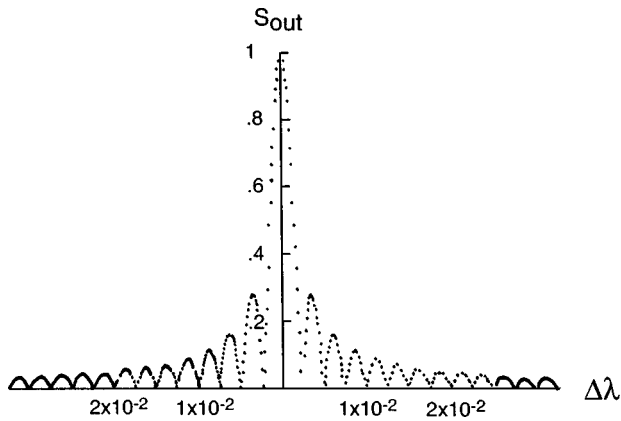


Fig. 15 Plot of S_{out} vs $\Delta\lambda$.

Figures 15 through 17 show, respectively, the variation of the amplitude of the output S beam as a function of the wavelength error, the output angular error, and its spatial distribution as a function of the output angles relative to the Bragg angle. Note that in Fig. 16, the overall output angle $\theta = \theta_B + \Delta\theta$ was used instead of the deviation from the Bragg direction. In the figure, the peak of the sinclike function is at the Bragg angle and the side lobes decrease steadily from there. The asymmetry in the plot is evidence of the nonlinearity of the relationship between output angular deviation and wavelength [Eq. (18)]. The mapping from $\Delta\theta$ to r' in Fig. 17 was accomplished simply by setting up the amplitude in the Bragg direction normal to the r' axis and plotting the other amplitudes around this in accordance with the deviation from the Bragg angle as per the results in Fig. 16. The final plot is multivalued and has multiple zeroes as in a typical radiation pattern polar plot simply because of the multiple zeroes versus angle as indicated by Fig. 16. To find the wavelength corresponding to the given amplitude and direction, we must measure the angular error for a given amplitude from Fig. 17, then find the corresponding wavelength error from Fig. 13. By using an analogous technique, the output spatial distribution relative to the Bragg direction for the S beam corresponding to a READ beam with a (more realistic) Gaussian wavelength spectrum is shown in Fig. 18. The standard deviation of the Gaussian is kept once again within 30% of the center wave-

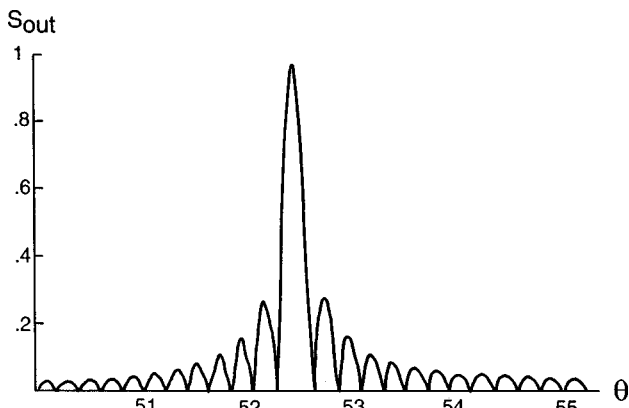


Fig. 16 Plot of S_{out} versus overall output angle θ .

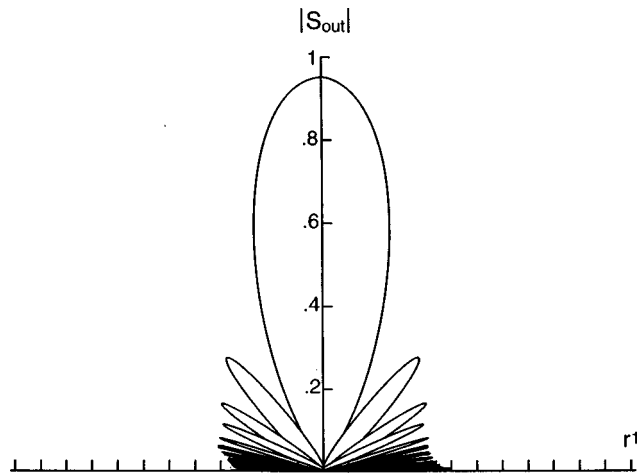


Fig. 17 Wavelength-dependent amplitude distribution plotted versus angle relative to the normal to the r' axis.

length ($1 \mu\text{m}$) in either direction. The scattered output in this case is very similar to that for the uniform spectrum except that the sinc function for the amplitude versus wavelength error is now delimited by a Gaussian envelope. We also observe that due to the increased attenuation at the outer ends of the Gaussian, fewer "loops" are in the pattern. Finally, a plot of efficiency versus wavelength error (assuming single, monochromatic, non-Bragg wavelengths only) is shown in Fig. 19 for $Q = 533$. From the plots over different Q , it may be shown that the range of $\Delta\lambda$ over which efficiency is an acceptable value narrows as Q increases. That is, the wavelength selectivity increases as Q increases. This, as seen earlier, is true for the efficiency as a function of input angular deviation as well. Thus, the parameter Q may be regarded as a measure of angular selectivity or wavelength selectivity.

5 Concluding Remarks

In this paper, we presented a study of the effects of angular misalignment and wavelength detuning on the performance of holographic gratings, initially using the acousto-optic Bragg grating as a model and then comparing the results for

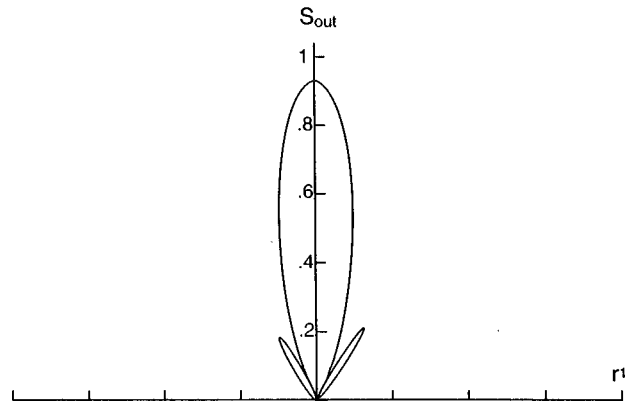


Fig. 18 Wavelength-dependent amplitude distribution for a Gaussian READ amplitude spectrum plotted versus angle relative to the normal to the r' axis.

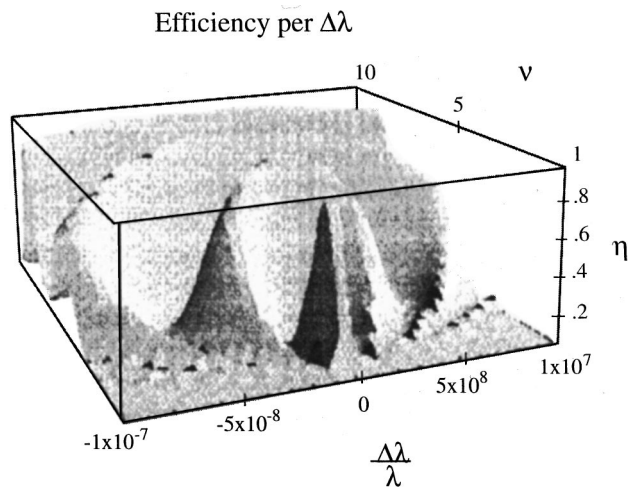


Fig. 19 Efficiency versus wavelength deviation for $Q=533$.

the two systems under profiled READ beams. The results compared favorably when the parameters of the holographic grating are tailored to match those of the A-O grating. The equivalence of the transfer function and Fourier transform formalism based on the A-O multiple plane wave scattering approach and Kogelnik's coupled wave theory also were demonstrated. The efficiency of a holographic grating under a uniform plane wave with angular misalignment were examined for different Q and the effect on the angular selectivity determined. A novel approach was developed to characterizing the output of a grating with regard to wavelength detuning (for which the transfer function or Fourier transform method is inadmissible). The output spatial distribution of the scattered order of light corresponding to a uniform and a Gaussian polychromatic READ beam spectrum was determined as a function of departure from the nominal Bragg direction. Finally, the efficiency of a holographic grating as a function of input wavelength detuning, was also investigated at different Q .

References

1. H. Kogelnik, "Coupled wave theory for thick hologram gratings," *Bell Syst. Tech. J.* **48**, 2909–2947 (1969).
2. C. W. Slinger and L. Solymar, "Grating interactions in holograms recorded with two object waves," *Appl. Opt.* **25**, 3283–3287 (1986).
3. H. Gerritson, D. Thornton, and S. Bolton, "Application of Kogelnik's two wave theory to deep, slanted, highly efficient relief transmission gratings," *Appl. Opt.* **30**, 807–814 (1991).
4. P. Leclere, Y. Renotte, and Y. Lion, "Measure of the diffraction efficiency of a holographic grating created by two Gaussian beams," *Appl. Opt.* **31**, 4725–4732 (1992).

5. K. Nonaka, "Diffraction efficiency analysis in hologram gratings recorded by counter-propagating type geometry," *J. Appl. Phys.* **78**, 4345–4352 (1995).
6. R. DeVrè, J. Heanne, K. Gürkan, and L. Hesselink, "Transfer functions based on Bragg detuning effects for image bearing holograms recorded in photorefractive crystals," *J. Opt. Soc. Am. A* **13**, 1331–1344 (1996).
7. S. Ahmed and E. N. Glytsis, "Comparison of beam propagation method and rigorous coupled-wave analysis for single and multiplexed volume gratings," *Appl. Opt.* **35**, 4426–4435 (1996).
8. H. Sasaki, K. Shinozaki, and T. Kamijoh, "Reduced alignment accuracy requirement, using focused Gaussian beams for free-space optical interconnection," *Opt. Eng.* **35**, 2240–2249 (1996).
9. M. R. Chatterjee, T.-C. Poon and D. N. Sitter, Jr., "Transfer function formalism for strong acousto-optic Bragg diffraction of light beams with arbitrary profiles," *Acustica* **71**, 81–92 (1990).
10. R. Magnusson and T. K. Gaylord, "Diffraction regimes of transmission gratings," *J. Opt. Soc. Am.* **68**, 809–814 (1978).
11. M. G. Moharam, T. K. Gaylord, and R. Magnusson, "Criteria for Raman-Nath regime diffraction by phase gratings," *Opt. Commun.* **32**, 19–23 (1980).
12. M. G. Moharam, T. K. Gaylord, and R. Magnusson, "Criteria for Bragg regime diffraction by phase gratings," *Opt. Commun.* **32**, 14–19 (1980).
13. P. P. Banerjee and T.-C. Poon, *Principles of Applied Optics*, Aksen Associates, Inc., Boston, MA (1991).
14. S.-T. Chen, "Analytical investigations of dynamic and static optical gratings and some modern applications," Ph.D. dissertation, Binghamton University, State University of New York (1997).



Monish R. Chatterjee received the B. Tech. degree in electronics and electrical communications engineering from the Indian Institute of Technology, Kharagpur, in 1979, and the M.S. and Ph.D. degrees in electrical engineering from the University of Iowa, Iowa City, in 1981 and 1985, respectively. After teaching for one year at the University of Iowa as a Visiting Assistant Professor, Dr. Chatterjee joined the electrical engineering department at Binghamton University, State University of New York, in 1986, where he is currently Associate Professor and Director of Graduate Studies. Dr. Chatterjee has published more than 20 papers in refereed journals and presented more than 60 papers at international conferences. His current research interests include holography, acousto-optics, and wave propagation. Dr. Chatterjee is a Senior Member of the IEEE and a member of the OSA, the ASEE, and Sigma Xi.



David D. Reagan received his BSEE and MSEE from Binghamton University in 1995 and 1998, respectively. He has been employed since 1997 at SYMTX, in Endicott, NY, as a member of the Technical Staff. At SYMTX, he is involved in the development of electronic and electro-optic test and measurement systems. His current fields of interest are optoelectronics, signal processing, and instrumentation.